Influence of nickel precursors on the properties and performance of Ni impregnated zeolite 5A and 13X catalysts in CO_2 methanation

Wei, Liangyuan; Haije, Wim; Kumar, Narendra; Peltonen, Janne; Peurla, Markus; Grenman, Henrik; de Jong, Wiebren

DOI
10.1016/j.cattod.2020.05.025

Publication date
2020

Document Version
Final published version

Published in
Catalysis Today

Catalysis Today 362 (2021) 35–46

Contents lists available at ScienceDirect

Catalysis Today

journal homepage: www.elsevier.com/locate/cattod

Influence of nickel precursors on the properties and performance of Ni impregnated zeolite 5A and 13X catalysts in CO_2 methanation

Liangyuan Wei[a], Wim Haije[a], Narendra Kumar[b], Janne Peltonen[c], Markus Peurla[d], Henrik Grenman[b,*], Wiebren de Jong[a,*]

[a] Faculty 3mE, Department of Process and Energy, Section Large-Scale Energy Storage, Delft University of Technology, Delft, the Netherlands
[b] Faculty of Science and Engineering, Johan Gadolin Process Chemistry Centre, Laboratory in Industrial Chemistry and Reaction Engineering, Åbo Akademi University, Turku/Åbo, Finland
[c] Department of Physics and Astronomy, University of Turku, Turku, Finland
[d] Laboratory of Electron Microscopy, University of Turku, Finland

ARTICLE INFO

Keywords:
Ni precursor salt anions
13X zeolite
5A zeolite
CO_2 methanation catalyst
Material properties
Catalytic performance

ABSTRACT

Zeolite 13X and 5A supported Ni catalysts were synthesized for CO_2 methanation using the evaporation impregnation method. The influence of using different Ni precursors (nitrate, citrate, and acetate) as well as calcination temperatures on the catalyst properties and performance were investigated. XRD, SEM-EDX, TEM, STEM-EDX, N_2 physisorption, H_2-TPR, TPD-NH_3 and TG/DTA were used for detailed characterization of the catalysts. The parent structure of the zeolites did not change during catalyst synthesis. Using nickel citrate and acetate resulted in smaller NiO particle size compared to nitrate. STEM-EDX results showed that all the Ni-precursor complexes entered more efficiently the 13X zeolite structure, which is mainly due to steric hindrance resulting from the smaller pore size of 5A. Methanation experiments revealed that the 13X catalysts synthesized using nickel citrate (5% Ni) displayed clearly higher activity, compared to the catalysts synthesized using nickel nitrate or nickel acetate. A 79% conversion at 320 °C was obtained with 100% selectivity towards CH_4 and the catalyst showed excellent stability during 200 h testing. Overall, it can be concluded that the Ni precursor significantly influences the physico-chemical characteristics and catalytic properties of Ni 13X and Ni 5A zeolite catalysts in CO_2 methanation: complex size and pore size matter.

1. Introduction

Decreasing carbon dioxide emissions is a crucial task for all countries, in order to limit the severe challenges arising from global warming [1,2]. Utilization of CO_2 to produce renewable energy carriers has attracted significant attention in the last few years. CO_2 can be converted to several synthetic fuels including methane (CH_4), methanol (CH_3OH) and further on to dimethyl ether (CH_3OCH_3) [3]. The availability of the raw materials CO_2 and H_2 in the future is a key factor in the large-scale production of synthetic fuel and chemicals. Large amounts of CO_2 can be currently obtained from industrial facilities such as, fossil fuel-burning power plants and plants with CCS technologies (like oxyfuel combustion, chemical-looping combustion and calcium looping) [3–5]. Technologies for capturing CO_2 directly from the air are being developed at an increasing pace [6]. Sustainable H_2 can be obtained from the splitting of water by electrolysis with sustainable electricity or from biomass gasification [7–9]. Hydrogen transport and storage are key factors for a H_2 based economy, especially for large scale industrial applications [10]. This work investigates the utilization of H_2 and CO_2 to produce CH_4 via the Sabatier reaction (1), which is a promising method for storing energy in large scale in a form directly usable in already existing infrastructure [11]. It has the potential to provide a new way of obtaining renewable completely carbon neutral CH_4 for stabilizing energy demand, provided that CO_2 can be efficiently captured from biomass derived gas sources and air in the future [12,13].

$$CO_2 + 4H_2 \leftrightarrow CH_4 + 2H_2O;\ \Delta H_r^0\ (298\ K) = -165\ kJ/mol \quad (1)$$

The Sabatier reaction is limited by equilibrium. Sorption enhanced CO_2 methanation by removing water from the reaction mixture has received increasing attention during the last years, since it could be used to enhance the yield beyond equilibrium, according to Le Chatelier's principle [14,15]. A CO_2 conversion of close to 100% was obtained by Walspurger et al. by using a commercial Ni catalyst mixed

* Corresponding authors.
E-mail addresses: henrik.grenman@abo.fi (H. Grenman), Wiebren.deJong@tudelft.nl (W. de Jong).

https://doi.org/10.1016/j.cattod.2020.05.025
Received 14 November 2019; Received in revised form 8 April 2020; Accepted 6 May 2020
Available online 11 May 2020

with a 4A zeolite adsorbent in CO_2 methanation [15]. Borgschulte et al. observed that the selectivity to CH_4 was enhanced if the pore size of the support was larger than 5 Å, and that the CO_2 overall conversion rate was reduced if the pore size was chosen to be smaller than 3 Å, because the CH_4 produced inside the pores could not leave the crystal [16]. In a follow-up paper, Delmelle et al. developed new catalysts for sorption enhanced CO_2 methanation by loading Ni on a 13X zeolite using the wet impregnation method with nickel nitrate hexahydrate. They pointed out that 5 wt% Ni/13X catalyst showed good performance and that it can be operated continuously two to three-fold longer than 5 wt % Ni/5A in sorption enhanced CO_2 methanation [17]. Also these observations are prone to some serious doubt. The double peak in TPR can equally well be due to two different Ni species, those inside and those outside the zeolite structure. TPR on the 5A sample only exhibits the low temperature TPR peak presumably because these particles are all outside the zeolite structure, having a diameter of 20 nm on average.

For CO_2 methanation, nickel is the most widely used metal due to its high activity, high CH_4 selectivity, relatively abundant availability and low price [18,19]. Nickel nitrate has an excellent solubility in water and it is easy to thermally decompose into NiO, which is why it is often used as the precursor for nickel catalysts [14,17]. It has been reported that NiO and SiO_2 form nickel silicate like species that are stabilized by a nickel citrate precursor [20]. This effectively prevented the nickel particles from sintering at high reaction temperature [20]. He et al. found that the use of nickel citrate precursor, compared to nickel nitrate precursor, could significantly strengthen the NiO-support (SBA-15) interaction resulting in comparatively smaller nickel particles with high dispersion [21]. Citrate complex precursors have obtained much attention in the synthesis of nanomaterials, where similar methodology as used in catalyst preparation e.g. the amorphous citrate process has been employed [22–24]. Additionally, Li et al. observed that nickel acetate-derived Ni-Ac-La/SiC catalysts can obtain a small and narrow Ni particle size distribution [25].

The final aim of our approach to the Sabatier reaction is the envisioned sorption enhancement to 100% conversion using a molecular sieve supported catalysts. 13X and 5A zeolites with low Si/Al ratios have the right properties as adsorbent materials for gases and liquids. The adsorption of CO_2 and the hydrophilic properties in 13X and 5A zeolites are attributed to the presence of surface silanol (Si-OH) groups. The use of zeolites as catalyst support brings also challenges to the synthesis and the use of the catalyst due to the possible diffusion limitations caused by the microporous structure and the obtained benefits must be compared to the possible disadvantages. This is why focus is placed on obtaining insight in the actual location, size and dispersion of the Ni particles and how precursors play a role herein. Furthermore dispersion will evidently play a role in selectivity and activity. The performance of the zeolite supported catalyst is here investigated in the absence of the sorption enhancement (saturated with water) in order for the results to be comparable with catalysts not possessing this advantage. A follow-up study will report on the sorption aspects related to pore occupancy of impregnated material and sorption capacity. The performance of the catalyst with and without the benefit of sorption enhancement can in this way be clearly demonstrated and the benefit of using these zeolites to reach yields surpassing the thermodynamic limitations be verified. However, the basis for the catalyst development must be an active catalyst even without equilibrium shift.

Based on literature findings, apart from the common nitrates, nickel citrate and nickel acetate are promising nickel precursors for obtaining a high dispersion and small particle size. 13X (FAU) and 5A (LTA) zeolites are porous catalyst supports that have sodalite cages (β) and super cages (α) [26–29]. Ni species can be located inside as well as outside these cages [30,31], depending on their size. Studies on the effect of different nickel precursors for preparing zeolite supported catalysts have so far been limited, especially related to sorption enhanced CO_2 methanation. What is more, the performance of Ni zeolite catalysts could be influenced by different nickel precursors and thermal treatment steps, since the dispersion of the active phases and the reducibility of oxide precursors are dependent thereupon [21,32,33].

The current study focuses on the effect of preparation parameters of Ni modified 13X and 5A zeolite catalysts, using the evaporation impregnation method. Evaporation impregnation was chosen as it is a commonly used and easily operable synthesis method with high reproducibility. However, it offers also flexibility to the synthesis by varying different parameters such as temperature, impregnation concentration and time, evaporation rate and as in the current work, the choice of metal precursor [17]. Nickel nitrate (Nit), nickel citrate (Cit) and nickel acetate (Ace) were used as nickel precursors for the synthesis of catalysts: 5%Ni13X-Nit, 5%Ni13X-Cit, 5%Ni13X-Ace, 5%Ni5A-Nit, 5%Ni5A-Cit and 5%Ni5A-Ace. After calcination, crystal structure, morphology, NiO particle size, surface area and pore volume were characterized by XRD, SEM-EDX, TEM, STEM-EDX (elemental mapping), nitrogen physisorption, H_2-TPR, TG/DTA. Additionally, NH_3-TPD was used to determine the acidity of catalysts, relating to the catalyst performance in CO_2 methanation. The activity and selectivity tests of the catalysts were carried out using lab scale fixed bed flow reactor systems, where the product gas composition was analyzed online with a gas chromatograph.

2. Experimental section

2.1. Catalyst preparation

The Ni modified 13X and 5A zeolite supports were prepared using the evaporation impregnation method with different Ni precursors (nickel nitrate, nickel citrate and nickel acetate). A nominal Ni-metal loading of 5% by mass was aimed for in the preparation of the zeolite catalysts. Nickel (II) nitrate hexahydrate ($Ni(NO_3)_2{\cdot}6H_2O$, 99%, Merck Millipore), nickel (II) citrate hydrate ($Ni_3(C_6H_5O_7)_2{\cdot}xH_2O$, 98 + %, Alfa Aesar) and nickel(II) acetate tetrahydrate ($Ni(OCOCH_3)_2{\cdot}4H_2O$, 98%, Sigma-Aldrich) were used as the three different Ni precursors. The nickel precursor was dissolved in 250 mL of distilled water in a flask. An equivalent of 5 g of 0.212 − 0.500 mm size (sieve fraction) 13X zeolite (Si/Al ≈ 1.5 (Table S. 2 (supplementary material)), Honeywell Fluka, The Netherlands) or 5A zeolite (Si/Al ≈ 1.0 (Table S. 2 (supplementary material)), Merck Millipore, The Netherlands) was dried at 100 °C overnight in an oven before it was added to the solution. The pH of the solution was measured by using a potentiometric pH meter during the process. It was observed that the pH of the solution decreased dramatically from 7.5 to 4.9 when nickel citrate hydrate dissolved in the solution, while it increased to 8.8 after 13X zeolite was mixed in the solution (Table S. 1, supplementary material). Meanwhile, the pH of other solutions with nickel nitrate and nickel acetate stayed around 7.3–7.4, and increased to 7.6–7.8 after the zeolite was mixed into the solution. The pH of the nickel citrate solution was around 5 due to the deprotonation of the hydroxyl group of the citrate ligand [34,35]. The protons are taken up by basic sites in the zeolite leading to an increased pH eventually.

In order to avoid mechanical wear of the zeolite particle, the rotator-evaporator was operated at low rotational speed, 10 rpm, for 24 h at room temperature. After the 24 h of catalyst synthesis, evaporation of the aqueous solution was carried out in the rotator-evaporator at 50 °C using a water jet vacuum pump. The catalyst was then dried at 100 °C overnight before calcination in a muffle oven.

The calcination temperature should be higher than 300 °C since the decomposition temperature of nickel nitrate is around 280 °C [36]. The influence of the calcination temperatures 300 °C, 350 °C, 400 °C, 450 °C, for the 5%Ni13X-Nit catalyst was studied. The catalysts were calcined using a stepwise procedure [17]. They were put in a muffle furnace in air. The first heating step was to 250 °C with 4.5 °C/min and then temperature was kept constant for 40 min. Then the sample was heated to its target value with 2.5 °C/min and held there for 3 h. The catalysts labelled as 5%Ni13X-Nit-300, 5%Ni13X-Nit-350 and 5%Ni13X-Nit-450,

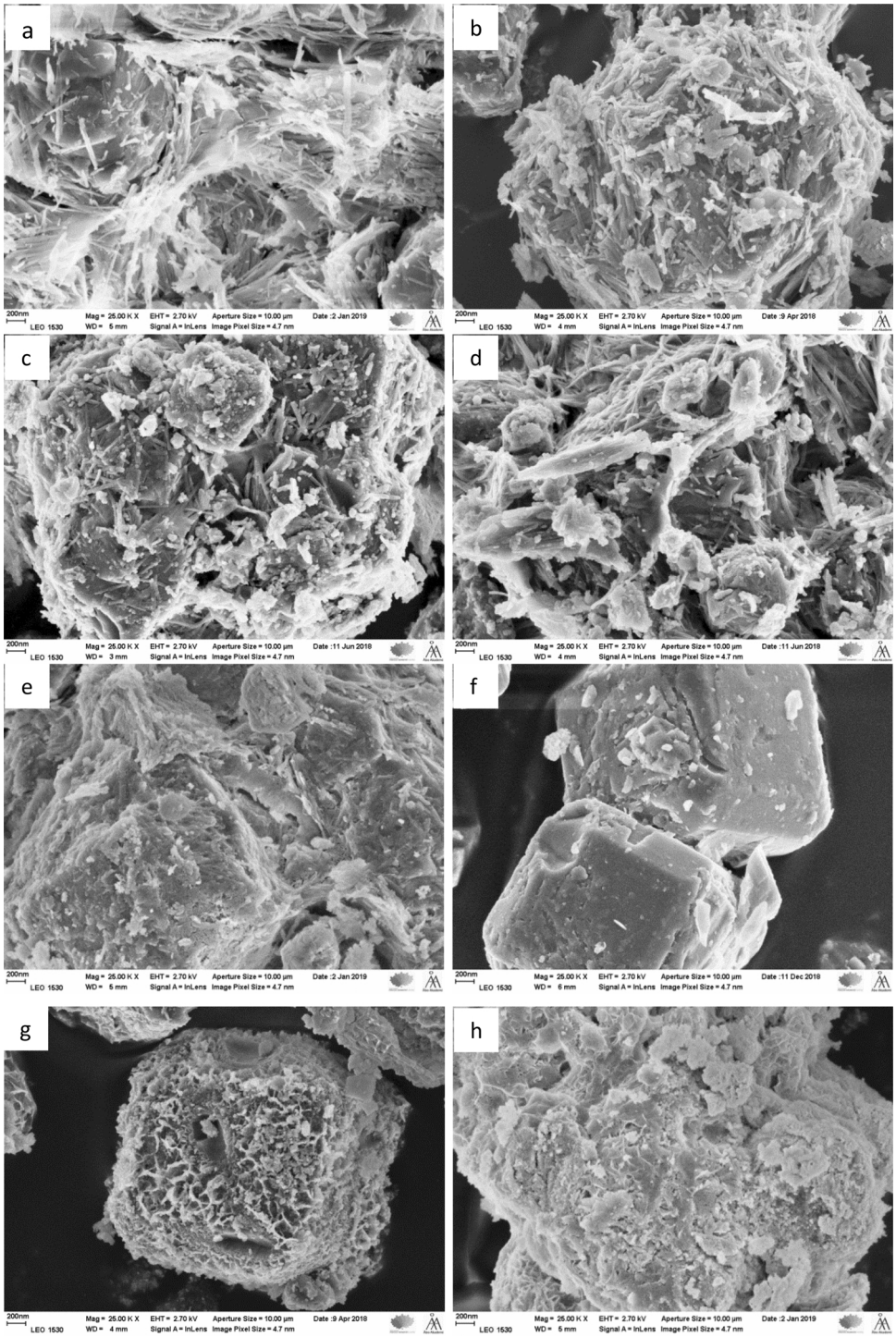

Fig. 1. SEM images of a fresh 13X zeolite, b 5%Ni13X-Nit, c 5%Ni13X-Cit, d 5%Ni13X-Cit-Spent, e 5%Ni13X-Ace, f fresh 5A zeolite, g 5%Ni5A-Nit and h 5%Ni5A-Ace (25,000×).

were calcined at the respective temperatures of 300 °C, 350 °C and 450 °C, respectively, all others only at 400 °C. Cooling down to room temperature took about 3 h.

2.2. Catalyst characterization

The calcined catalysts were characterized before reduction by X-ray powder diffraction (XRD), scanning electron microscopy (SEM), energy dispersive X-ray spectroscopy (EDX), transmission electron microscopy (TEM), scanning transmission electron microscopy equipped with energy-dispersive X-ray spectroscopy (STEM-EDX), nitrogen physisorption, hydrogen temperature programmed reduction (H_2-TPR), and temperature programmed ammonia desorption (NH_3-TPD).

A PANalytical Empyrean X-ray powder diffractometer was used in the XRD measurements. The diffractometer was operated in Bragg-Brentano diffraction mode, and the monochromatized Cu-Kα radiation ($\lambda = 1.541874$ Å) was generated with a voltage of 45 kV and a current of 40 mA. The scanning 2θ angle range was 3.0° to 80.0° using a step size of 0.013°, and counting time of 80 s /step. The measured XRD diffractograms were analyzed with Philips X'Pert HighScore (phase

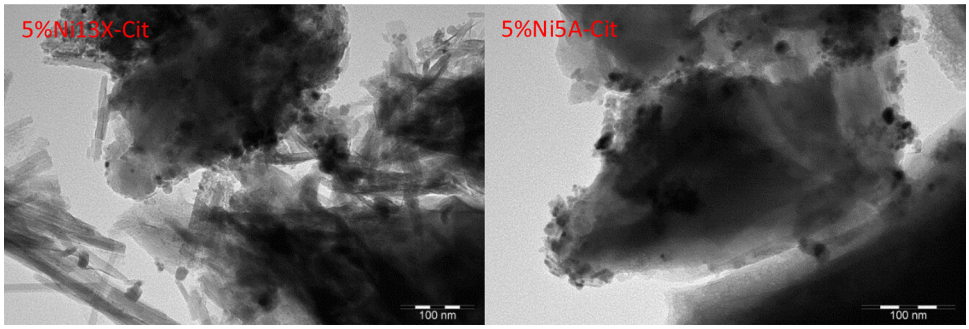

Fig. 2. Transmission electron micrographs of calcined 5%Ni13X -Cit, 5%Ni5A-Cit catalysts with nickel citrate precursors.

analysis refinement) and MAUD software programs (background subtraction).

Catalysts morphology, such as shape, size and size-distributions of crystals were studied using a LEO Gemini 1530 (LEO/ZEISS, Germany) Scanning electron microscope (SEM). The near surface elemental analysis was carried out by energy dispersive X-ray micro-analyses (EDX).

Transmission electron microscopy (TEM) was used to study the zeolite morphology and Ni- particle size distributions. The Ni-, particle size and the average particle size was calculated. The equipment used was JEM-1400(JEOL Ltd, Japan) with a maximum acceleration voltage of 120 kV.

To study the catalysts in more detail, scanning transmission electron microscopy equipped with an energy-dispersive X-ray spectroscopy (STEM-EDX) detector was used. The equipment used was a FEI Titan 80-300 electron microscope, the elemental mapping was investigated at a voltage of 300 kV with EDX. Specimen preparation consisted of immersing a carbon film supported on a copper grid into the catalysts powder, small particles adhering to the carbon film were measured.

The surface area and pore size of pristine 13X zeolite, Ni- modified 13X zeolite catalysts were measured using the nitrogen adsorption and similarly for the 5A counterpart. The instruments used were a Carlo Erba Sorptomatic, Sorptometer 1900 and Micromeretics, Tristar II. The catalysts were outgassed at 150 °C for 3 h at 8 mbar, prior to the surface area measurement. The calculation of surface area was carried out using the BET method.

Temperature programmed reduction (H_2-TPR) was carried out using a Micromeritics AutoChem 2910; The catalysts were dried at 250 °C for 1 h in a dry Ar atmosphere, then reduced by 5% H_2 (diluted by Ar) from room temperature to 900 °C with a 5 °C/min heating rate. A TCD detector was used to monitor the H_2 consumption.

Temperature programmed desorption of ammonia was carried out using a Micromeritics AutoChem 2910 for determining the acidic properties such as the amount of weak, medium, and strong acid sites and total amount of acid sites of the pristine forms of 13X, 5A and Ni-modified 13X and 5A zeolite catalysts. The samples were dried at 250 °C for 0.5 h in a dry He atmosphere before ammonia adsorption (5% NH_3 diluted by He) at room temperature, the desorption temperature ranged from 100 to 900 °C.

In order to investigate the catalysts calcination, thermogravimetric/differential thermal analyses (TG/DTA) were performed on SDT Q600 V20.9 Build 20 (TA Instruments) under 50 mL/min air atmosphere. The stepwise procedure of temperature in TG/DTA measurement was the same as the one for catalyst calcination above.

2.3. Catalysts test in fixed bed reactor

The catalysts' activity, selectivity and stability were tested using a fixed bed reactor made of quartz with an inner diameter of 10 mm. About 10 mL of silica beads (diameter around 1 mm) was placed in the reactor to support the catalyst bed. Then about 10 mL of silica beads was used to fill the upper part of the reactor. The reactor was heated by a vertical tube furnace equipped with a K-type thermocouple, while the temperature of the catalyst bed was monitored by another K-type thermocouple, which was inserted into the lower part of the catalyst bed and connected to a computer for data acquisition. A schematic representation of the fixed bed reactor system is displayed in Fig. S. 1 (supplementary material).

Before the experiments, around 0.9 g of the calcined catalyst was loaded into the reactor and reduced under 100 mL/min H_2 atmosphere at 500 °C for 4 h. The reduction temperature was selected based on the results obtained with catalysts reduced at different temperatures. It was observed that catalysts reduced at 500 °C (100 mL/min H_2) were more active in CO_2 methanation compared to the ones calcined at lower or higher temperature (Fig. S. 2, supplementary material). The catalysts activity tests were performed at temperatures between 240 °C and 440 °C with a gas hourly space velocity of 13333 mL/$g_{cat.}$/h. The feed mixture consisted of 40 mL/min H_2 and 10 mL/min CO_2 diluted by N_2 (150 mL/min). The product gas from the reactor was led through a cooling condenser and then analyzed using micro gas chromatography (GC). The GC (Varian, CP-4900 Micro-GC) equipped with HayeSep A, molecular sieve columns (Molsieve 5 Å PLOT) and a thermal conductivity detector. Helium was used as the carrier gas.

The CO_2 conversion (2) and catalyst selectivity (3) forwards CH_4 were defined as [37,38]:

$$X_{CO_2} = \frac{n_{CO_2,in} - n_{CO_2,out}}{n_{CO_2,in}} \quad (2)$$

$$S_{CH_4} = \frac{n_{CH_4,out}}{n_{CO_2,in} - n_{CO_2,out}} \quad (3)$$

where $n_{CO_2,in}$ is the input molar flow rate of CO_2 in the experiment, $n_{CO_2,out}$ and $n_{CH_4,out}$ are the molar flow rates of CO_2 and CH_4, respectively, calculated from GC results.

3. Results and discussion

3.1. Catalyst characterization

3.1.1. X-ray powder diffraction(XRD)

The XRD background corrected diffractograms for calcined Ni modified 13X and 5A zeolite catalysts with different Ni precursors are shown in Fig. S. 3 (supplementary material). The XRD patterns indicate that the crystal structure of 13X (cubic Faujasite) zeolite is maintained after the modification by precursors nickel nitrate, nickel citrate and nickel acetate. Similarly, the crystal structure of 5A (cubic) zeolite did not change after the modification by nickel nitrate. The peaks for NiO cannot be distinguished in the XRD patterns. This could be due to a too low amount of NiO peaks overlapping with those from the zeolites, or the presence of NiO as amorphous or nano sized material leading to peak broadening [39].

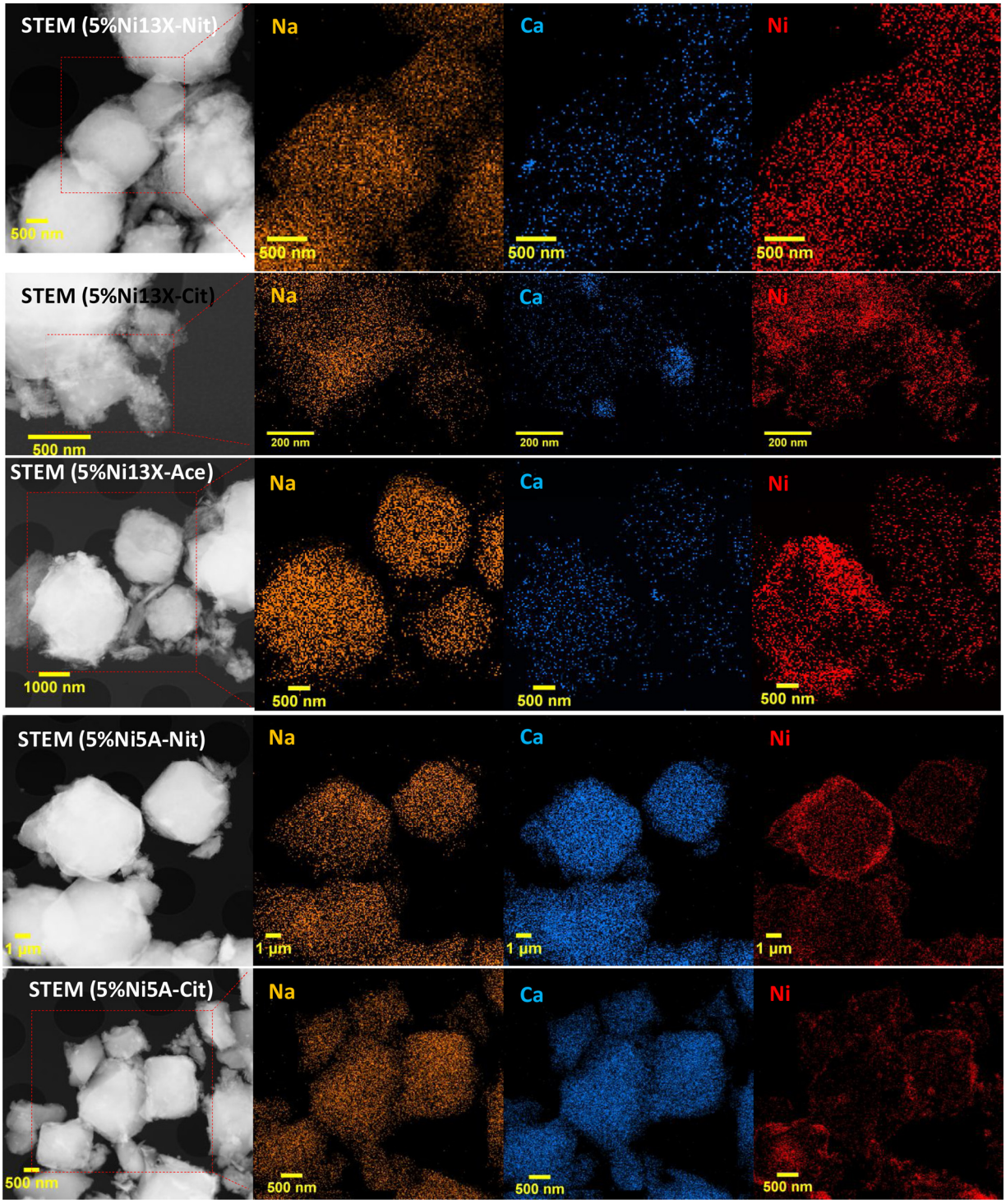

Fig. 3. STEM images (left pictures), Na (gold), Ca (light blue) and Ni (red) maps of Ni-zeolite catalysts with different Ni precursors (For interpretation of the references to colour in this figure legend, the reader is referred to the web version of this article).

3.1.2. Scanning electron microscopy (SEM) and Energy dispersive X-ray spectroscopy (EDX)

SEM was used to investigate the morphology of pristine (fresh) 13X and 5A zeolites and Ni modified 13X and 5A zeolite supported catalysts. Scanning electron micrographs of fresh 13X and 5A zeolites are shown in Fig. 1. The 13X zeolite showed relatively large agglomerates (around 2 µm) which are composed of its characteristic smaller fibrous crystals [17], while 5A zeolite showed regular cubic crystals with more distinct edges. The crystal morphology of a spent sample, e.g. 5%Ni13X-Cit-Spent was also similar to that of fresh 5%Ni13X-Cit, clearly indicating that the CO_2 methanation reaction did not alter it.

EDX results for catalysts are shown in Table S. 2 (supplementary material). It can be observed that the actual loading of Ni varies slightly for the different nickel precursors. The Ni content was 3.16% mass for the catalyst 5%Ni13X-Nit, and 3.52% mass for 5%Ni-13X-Cit. The Na and Ca content is very different for the fresh 13X and 5A zeolites which is reflected in the Ni modified 13X and 5A zeolite catalysts [40,41]. The presence of Ca, Mg and Na in the fresh (pristine) 13X, 5A, Ni- modified 5A and 13X (Table S. 2) contributes to the formation of basic sites in line with the increase of the pH during the impregnation process.

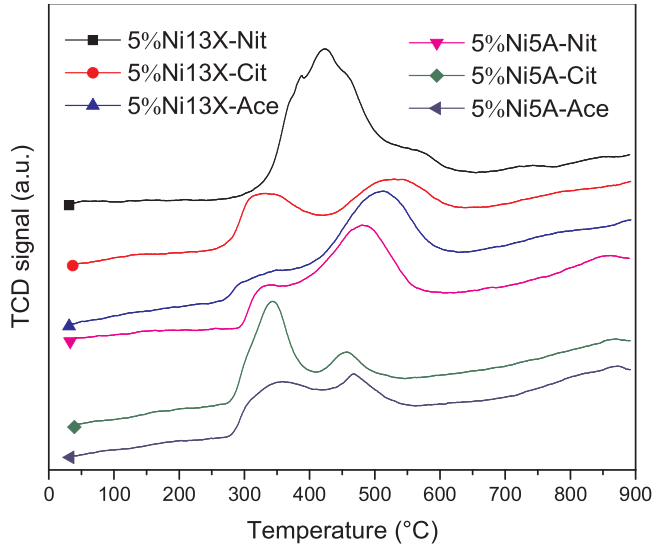

Fig. 4. H_2-TPR profiles of Ni-zeolite catalysts with different Ni precursors.

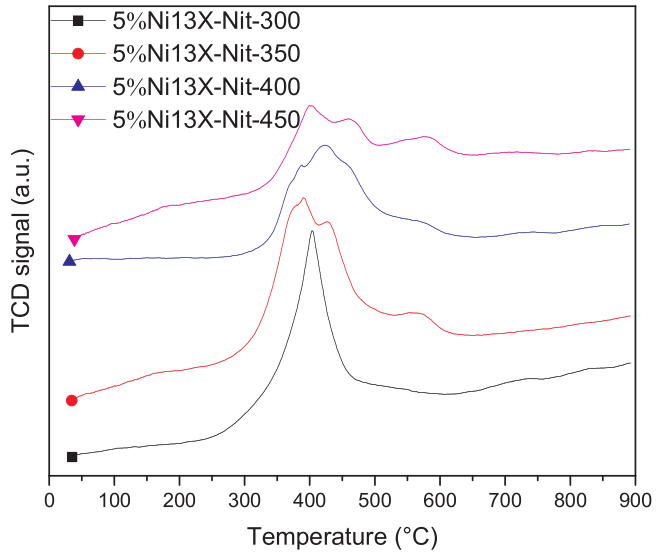

Fig. 5. H_2-TPR profiles of Ni-zeolite catalysts with different calcination temperatures.

3.1.3. Transmission electron microscopy (TEM)

TEM was used to investigate the NiO particle size distribution. Moreover, the textural properties of the fresh and calcined Ni modified 13X and 5A zeolites, their morphology and structure, were investigated. The TEM images of 5%Ni13X-Cit and 5%Ni5A-Cit prepared by nickel citrate are shown in Fig. 2 (TEM figures for other catalysts can be found from Fig. S. 4 (supplementary material)). The TEM images show the characteristic uniform structures of 13X and 5A zeolite, as well as the dispersed NiO particles on the external surface of 13X and 5A zeolite framework. It can again be observed from the TEM results that the Ni precursors (nickel nitrate, nickel citrate and nickel acetate) did not influence the morphology of 13X and 5A zeolite.

There are clearly two different kinds of particles present in the sample, lumpy ones, presumably resulting from the precipitation during the drying step in the impregnation procedure, and very small and well dispersed ones aimed for by the impregnation process. The lumpy ones are too big, tens of nm, to fit inside the pores of the zeolites. The chelating capacity of citrate and acetate is probably leading to the smaller size as compared to nitrate [20,42]. Furthermore it has been reported that nickel citrate may leave a highly viscous, adhering film on the surface which breaks up and decomposes during calcination, resulting in a large amount of small NiO particles [39,43].

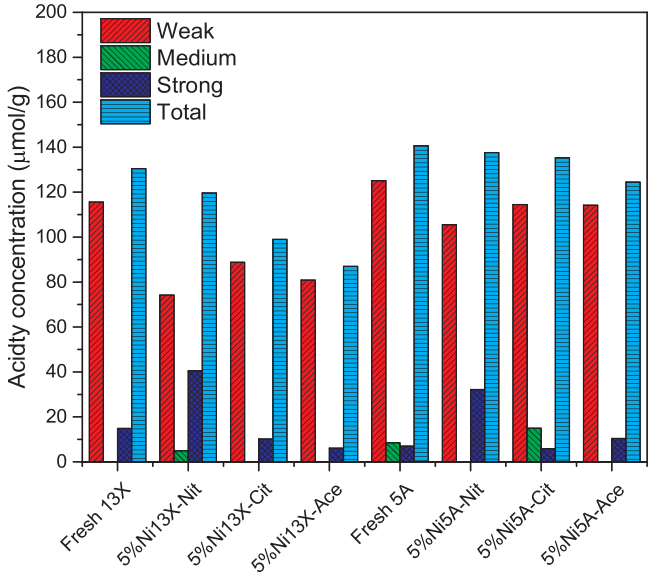

Fig. 6. The catalyst acidity distribution calculated based on the results of NH_3-TPD.

3.1.4. STEM-EDX

The STEM micrographs depicted in Fig. 3 show the NiO dispersion on and partly in the catalysts. The NiO dispersion is influenced by the properties of the support, e.g. the structure, pore size and crystal size of the zeolite and the precursor. Very small nano Ni (after reduction) particles ($< 1-2$ nm) are invisible in these TEM images, but still show high catalytic activity in reactions, due to their high surface free energy [44]. To further investigate the dispersion of the Ni (NiO) particles in 5A and 13X zeolite based catalysts, elemental mapping was carried out using STEM, equipped with EDX Micro -Analysis (STEM-EDX).

The STEM elemental mappings, Na (gold), Ca (blue) and Ni (red), of Ni-zeolite catalysts with different Ni precursors are shown in Fig. 3. Ni is rather well dispersed on and in 13X zeolite for nickel nitrate, nickel citrate and nickel acetate precursors, however, the smallest Ni clusters can be clearly observed for the catalyst synthesized with the citrate precursor. The 5%Ni5A-Nit and 5%Ni5A-Cit catalyst, have predominantly Ni on the cubic crystal outside surface of 5A zeolite in an eggshell fashion (Fig. 3), this “eggshell” could correspond to the smaller crystallites or particles observed from SEM results of Ni 5A catalysts (Fig. 1). Clearly the precursors were too big to enter the 5A pores, as is further indicated by the deviating more homogeneous distribution of Ca and Na.

3.1.5. Nitrogen physisorption

The specific surface area of fresh zeolites and catalysts was determined using nitrogen adsorption. The surface area of 13X and 5A was determined to be 685 m^2/g and 692 m^2/g, respectively. After the Ni modification, the catalysts had a lower surface area compared to the fresh 13X and 5A zeolites (See supplementary material Table S. 4). A plausible reason for decrease in the surface area is pore blocking. For the 13X based catalysts, it is especially noteworthy that the surface area decreased significantly less when the citrate precursor was used. For the more efficient 13X supported catalyst the surface area dropped from 685 m^2/g to 611 m^2/g with citrate precursor while 361 m^2/g was obtained with the nitrate precursor. The observed decrease in surface area was not as great with the 5A supported catalysts when nitrate was used, which supports the observation made with STEM-EDX that the nickel precursors did not penetrate the pores of the 5A efficiently. The external

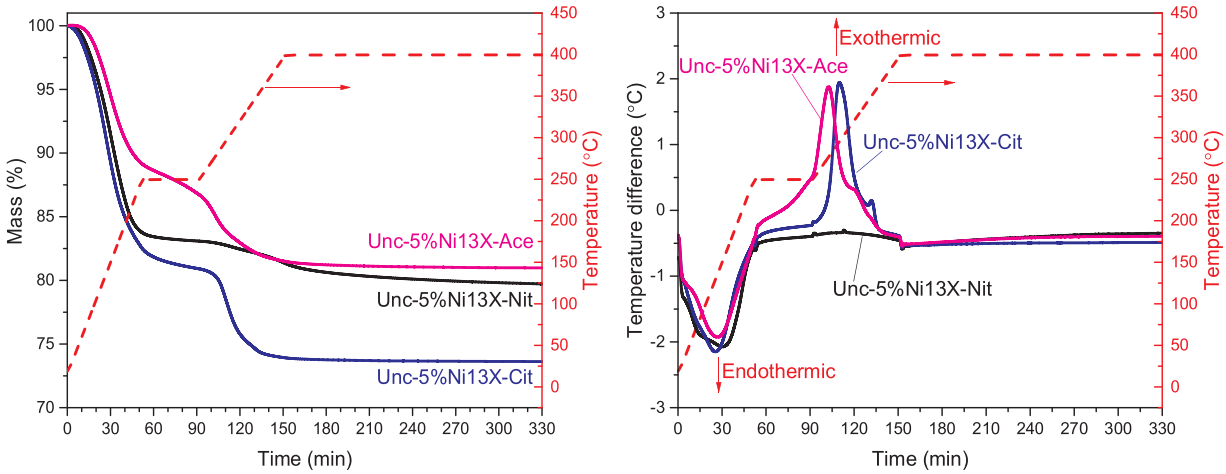

Fig. 7. TG/DTA curves during thermal calcination under air for uncalcined Ni 13X samples prepared using nickel nitrate, nickel citrate and nickel acetate.

Table 1
Analysis summary of the TG/DTA results in Fig. 7.

Sample	First mass loss[a]		Second mass loss[b]		Total mass loss wt.%
	Mass loss wt.%	Peak °C	Mass loss wt.%	Peak °C	
Unc-5%Ni13X-Nit	16.92	150	3.36	301	20.28
Unc-5%Ni13X-Cit	19.09	140	7.29	300	26.38
Unc-5%Ni13X-Ace	13.23	148	5.79	279	19.02

[a] Mass loss from room temperature to end of 250 °C.
[b] Mass loss from 250 °C to end of 400 °C.

surface area of the parent zeolites was determined from the t-plots to be 44 m^2/g and 45 m^2/g for 13X and 5A, respectively. It can be concluded that external surface area does not explain the differences observed between the zeolites. The impregnation did not influence significantly the external surface area e.g. it decreased for the most efficient 5% Ni13X-cit from 44 to 40 m^2/g. The surface area measurements support the observations made with STEM-EDX. The Ni was deposited mainly on the external surface of 5A zeolite while for 13X, the nickel precursor is able to more efficiently penetrate into the pores of zeolite. Moreover, the use of nickel citrate seems to results in smaller clusters inside the pores of zeolite resulting in retaining a higher surface area.

3.1.6. H_2-Temperature programed reduction (TPR)

The TPR profiles of Ni-zeolite catalysts prepared by different Ni precursors and different calcination temperatures are displayed in Figs. 4 and 5. The reduction behavior of the catalyst and the relative H_2 consumption can be found in Table S. 5 (supplementary material). It can be seen that with increasing calcination temperature the TPR signal evolves from a quasi-single peak to a broad band of peaks extending to higher reduction temperature. For the catalysts prepared by different Ni precursors (Fig. 4), 5%Ni13X-Nit shows a wide and intense peak at around 420 °C, while all the others have two peaks in the same temperature range, one appearing at around 330 − 350 °C and another at around 460 − 530 °C. This may indicate that different Ni precursors result in Ni oxides being formed at different reduction sites on or in the zeolite cages. The peak at 330 − 350 °C could correspond to NiO particles located outside of the zeolite cages and are more easily reduced, while the peak at 460 − 530 °C may correspond with NiO particles located within the zeolite super cages [30,31,45]. The reduction peaks of 5%Ni13X-Cit and 5%Ni5A-Cit at around 340 °C are strong, which indicates that more Ni oxides were located outside the 13X and 5A zeolite cages, compared to the catalysts prepared from nickel nitrate and nickel acetate.

The diameter of the $Ni^{2+}(H_2O)_x$ ion [46,47] is similar or bigger than the pore diameter of 13X zeolite (7.4 − 11 Å) [17,48,49] and 5A zeolite

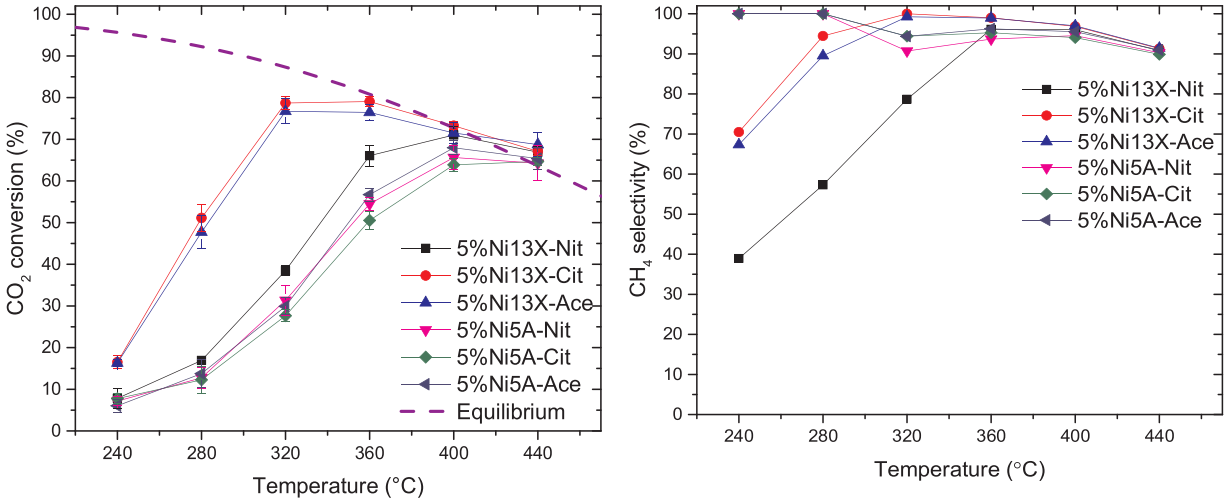

Fig. 8. CO_2 conversion (left) and CH_4 selectivity (right) using catalysts with different Ni precursors (reduction at 500 °C, 4 h), 0.9 g, 150 mL/min N_2, 40 mL/min H_2, 10 mL/min CO_2.

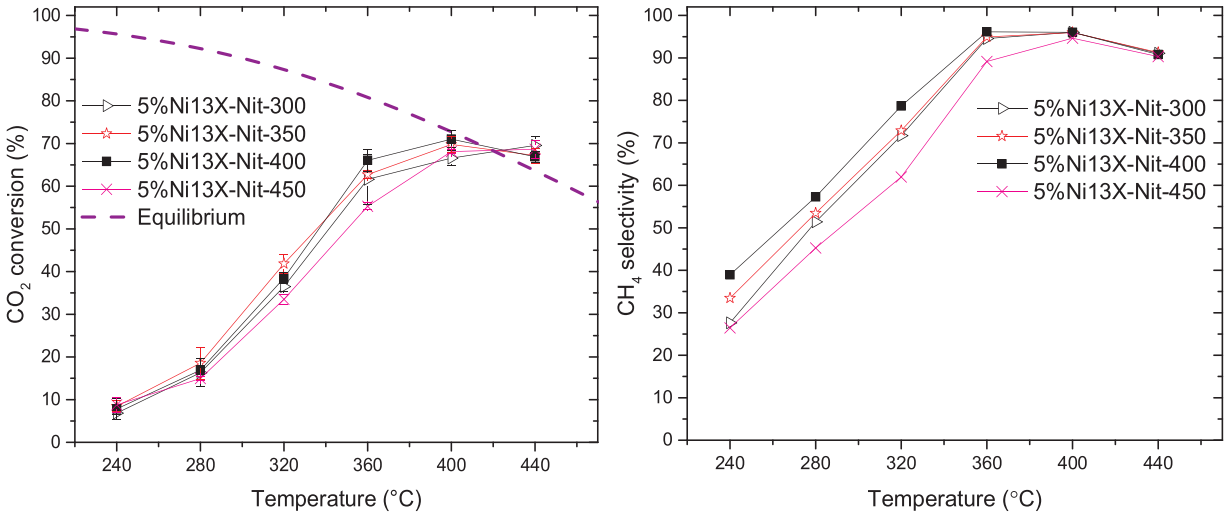

Fig. 9. CO_2 conversion (left) and CH_4 selectivity (right) using catalysts with different calcination temperatures (reduction at 500 °C, 4 h), 0.9 g, 150 mL/min N_2, 40 mL/min H_2, 10 mL/min CO_2.

(4.3 − 5 Å) [17,49]. Nickel citrate and acetate complexes (especially the nickel citrate complexes) are both too big to enter zeolite 5A but may enter zeolite 13X during the catalyst preparation [50]. This is also a plausible reason why Ni was predominantly found on the surface of 5A cubic crystals (Fig. 3) as compared to the 13X particles.

The calcination temperature seems to influence the NiO reduction property significantly (Fig. **5**). A very sharp and strong reduction peak is observed for 5%Ni13X-Nit-300, which was calcined at 300 °C, while the catalysts calcined at higher temperature display a weaker and broader peak at around 400 °C and another at around 570 °C. Thus a higher calcination temperature results in clustered or sintered NiO particles located in the 13X cages.

3.1.7. Temperature programmed desorption of ammonia (NH_3-TPD)

The acidic properties of Ni-modified 13X and 5A zeolite catalysts were studied using temperature programmed desorption of NH_3-TPD. The comparisons of the pristine proton forms 13X and 5A zeolite supports were carried out with those of Ni-modified 13X and 5A zeolite catalysts. The most notable observation was that the total acidity only changed little, weak acidity is similar for all samples, medium acidity is virtually absent for the 13X series and the strong acidity is similar for all. On the whole, the 5A derived catalysts are more acidic than the 13X counterparts. The low temperature peaks are attributed to the Lewis acid sites and high temperature peaks (400 − 600 °C) are attributed to the Brønsted acid sites. Some peaks were also observed in the temperature range of 600 − 800 °C, these peaks are attributed to extra-framework aluminum species (Al-OH), $(Al\text{-}OH)_2$ and silanol groups (SiOH), $(SiOH)_2$. The extra-framework silanol groups are formed due to dehydroxylation reaction at high temperature (600 − 800 °C).

The catalyst acidity distribution calculated by the results of NH_3-TPD is shown in Fig. 6 (NH_3-TPD profiles and detailed calculation results can be found from supplementary material Fig. S. 5 and Table S. 3.). The type of nickel precursor used for the synthesis of Ni modified 13X and 5A zeolite catalysts was observed to influence the total acidity only slightly, but there is a trend when looking in detail. The 5%Ni13X-Nit catalyst prepared using nickel nitrate aqueous solution exhibited highest total acidity. The total acidity of the Ni- modified catalysts followed the pattern: 5%Ni13X-Nit > 5%Ni13X-Cit > 5%Ni13X-Ace. The 5%Ni5A-Nit catalyst showed the highest total acid sites (137 μmol/g). The amount of total acid sites for Ni modified 5A zeolite catalyst followed the similar pattern as that of Ni modified 13X zeolite.

3.1.8. Thermogravimetric/differential thermal analyses (TG/DTA)

The TG/DTA was performed to investigate zeolite supported catalysts' calcination behavior, the results are shown in Fig. 7. It can be observed that the mass of the samples is close to constant after 3 h of calcination under air atmosphere at 400 °C. There are two main mass loss stages with the temperature increase. One is from room temperature to 250 °C, which corresponds to the desorption of water and other gases in zeolite 13 × . This was followed by another main mass loss after 250 °C for the three samples, which corresponds to the decomposition of nickel nitrate [51], off-burning nickel citrate [52] and off-burning nickel acetate salt (or their intermediates) [53]. It was observed that the mass loss of Unc-5%Ni13X-Cit and 5%Ni13X-Ace in the second stage is much more severe than 5%Ni13X-Nit (Fig. 7), and the mass loss of 5%Ni13X-Nit is less than the others (Table 1). This is due to the different decomposition reactions of the Ni precursors. The very sharp exothermic burning stage (second peak) of Unc-5%Ni13X-Cit and Unc-5%Ni13X-Ace can be observed from Fig. 7, while Unc-5%Ni13X-Nit did not have the exothermic stage.

3.2. Experiments for catalysts performance on CO_2 methanation in a fixed bed reactor

3.2.1. Catalyst activity and selectivity

Ni- modified 13X and 5A zeolite catalysts activity and selectivity were tested in a lab scale fixed bed reactor system, and the results are shown in Figs. 8 and 9. The catalyst performance comparison with the results from literatures can be found in Table 2.

The CO_2 conversion at each temperature was the average value based on GC measurements for five times, which were stable after the zeolite absorbed some water under the experimental condition. The error bars in these figures show that all test results have a good reproducibility. As the catalyst was already saturated with water before activity and selectivity data was taken, adsorption enhancement can be excluded from the data. The thermodynamic equilibrium conversion of CO_2 was calculated to compare with the performance of the catalysts. It can be observed, that the CO_2 conversion is very close to the equilibrium value for most catalysts at 440 °C and for the most active catalysts rather close even at 320 °C. As the sorption enhancement effect of the zeolites was intentionally suppressed in this study to obtain comparable results with other catalysts, e.g. the conversion of the most active catalysts decreases after 320 °C due to the thermodynamic limitations. Moreover, all the curves of CO_2 conversion in Fig. 8 show a similar trend with increasing temperature, as the conversion increases dramatically from below 20% to near equilibrium followed by a decrease due to equilibrium limitations. The reaction is limited by kinetics at low temperature [14] and by thermodynamics at high temperatures

Table 2
Catalysts performance comparison with the results from literature sources.

Catalyst[a]	NiO or Ni particle size (nm)	Reactor diameter (mm)	Catalyst size (mm)	Catalyst for test (g)	H_2/CO_2/Inert gas ratio	Total flow (ml/min) (exp. pressure)	GHSV Or WHSV	CO_2 Conversion (%)	CH_4 Selectivity (%)	Rate (mol_CO_2/mol_Ni/s)[b]	Activation energy (kJ/mol)	Ref.
5%Ni13X-Nit	12.3	10	0.212 − 0.5	0.9	4:1:15	200 (1 bar)	13,333 ml/g/h	7.8 (240 °C) 16.9 (280 °C)	38.9 (240 °C) 57.3 (280 °C)	0.0030 0.0066	56[c]	This work
5%Ni13X-Cit	11.5	10	0.212 − 0.5	0.9	4:1:15	200 (1 bar)	13,333 ml/g/h	16.5 (240 °C) 51.1 (280 °C)	70.5 (240 °C) 94.5 (280 °C)	0.0064 0.0198	29 [c]	This work
5%Ni13X-Ace	5.2	10	0.212 − 0.5	0.9	4:1:15	200 (1 bar)	13,333 ml/g/h	16.3 (240 °C) 47.7 (280 °C)	67.3 (240 °C) 89.5 (280 °C)	0.0063 0.0185	32 [c]	This work
5%Ni5A-Nit	9.7	10	0.212 − 0.5	0.9	4:1:15	200 (1 bar)	13,333 ml/g/h	7.2 (240 °C) 12.8 (280 °C)	100 (240 °C) 100 (280 °C)	0.0028 0.0050	61 [c]	This work
5%Ni5A-Cit	6.3	10	0.212 − 0.5	0.9	4:1:15	200 (1 bar)	13,333 ml/g/h	7.8 (240 °C) 12.3 (280 °C)	100 (240 °C) 100 (280 °C)	0.0030 0.0048	55 [c]	This work
5%Ni5A-Ace	5.7	10	0.212 − 0.5	0.9	4:1:15	200 (1 bar)	13,333 ml/g/h	6.0 (240 °C) 13.8 (280 °C)	100 (240 °C) 100 (280 °C)	0.0023 0.0054	53 [c]	This work
5%Ni13X-Nit-300	_	10	0.212 − 0.5	0.9	4:1:15	200 (1 bar)	13,333 ml/g/h	6.8 (240 °C) 16.3 (280 °C)	27.6 (240 °C) 51.4 (280 °C)	0.0026 0.0063	55 [c]	This work
5%Ni13X-Nit-350	13.5	10	0.212 − 0.5	0.9	4:1:15	200 (1 bar)	13,333 ml/g/h	8.4 (240 °C) 18.5 (280 °C)	33.5 (240 °C) 53.5 (280 °C)	0.0033 0.0072	56 [c]	This work
5%Ni13X-Nit-450	11.6	10	0.212 − 0.5	0.9	4:1:15	200 (1 bar)	13,333 ml/g/h	8.8 (240 °C) 14.9 (280 °C)	26.4 (240 °C) 45.3 (280 °C)	0.0034 0.0058	55 [c]	This work
5%Ni/MSN	9.9	8	0.2 − 0.4	0.2	4:1:0	167 (1 bar)	50,000 mL/g/h	82 (350 °C)	99.9 (350 °C)	0.1196	76	[56]
5%NiUSY	–	–	–	–	36:9:10	250 (1 bar)	43,000/h	2.2 (250 °C) 9.4 (300 °C)	– –	0.0048	_	[54]
5%NiUSY	17 − 33	–	–	–	36:9:10	250 (1 bar)	43,000/h	2.1 (250 °C) 6.7 (300 °C)	99.4 (250 °C) 93.1 (300 °C)	0.0205	_	[30]
20%Ni/SiO_2	21.1	9	0.07 − 0.59	0.2	76:19:5	33 (1 bar)	10000 mL/g/h	41 (350 °C)	89 (350 °C)	0.0046	_	[57]
5%NiMSN	9.9	8	0.02 − 0.04	0.2	4:1:0	167 (1 bar)	50000 mL/g/h	64.1 (300 °C)	99.9 (300 °C)	0.0146	_	[58]
5%Ni/MCM-41	10.5	8	0.02 − 0.04	0.2	4:1:0	167 (1 bar)	50000 mL/g/h	56.5 (300 °C)	98.3 (300 °C)	0.0030	_	[58]
5%Ni/HY	19.8	8	0.02 − 0.04	0.2	4:1:0	167 (1 bar)	50000 mL/g/h	48.5 (300 °C)	96.4(300 °C)	0.0935	76	[58]
5%Ni/SiO2	17.8	8	0.02 − 0.04	0.2	4:1:0	167 (1 bar)	50000 mL/g/h	42.4 (300 °C)	96.6 (300 °C)	0.0824	78	[58]
5%Ni/γ-Al_2O_3	–	8	0.02 − 0.04	0.2	4:1:0	167 (1 bar)	50000 mL/g/h	27.6 (300 °C)	95.2 (300 °C)	0.0707	81	[58]
20%Ni/Al_2O_3	> 10	–	0.212 − 0.25	0.7	6:30:64	750 (1 bar)	55,000/h	20 (300 °C)	99.8 (300 °C)	0.0618	84	[59]
10%Ni/H-Y	17.0	9	0.3 − 0.5	0.5	4:1:1.25	250 (1 bar)	10,000/h	15 (350 °C)	88 (350 °C)	0.0403	103	[60]
10%Ni/Na-Y	19.8	9	0.3 − 0.5	0.5	4:1:1.25	250 (1 bar)	10,000/h	30 (350 °C)	82 (350 °C)	0.0094	_	[60]
10%Ni/H-BETA	19.1	9	0.3 − 0.5	0.5	4:1:1.25	250 (1 bar)	10,000/h	23 (350 °C)	88 (350 °C)	0.0066	_	[60]
10%Ni/Na-BETA	20.1	9	0.3 − 0.5	0.5	4:1:1.25	250 (1 bar)	10,000/h	33 (350 °C)	88 (350 °C)	0.0131	_	[60]

[a] HY or H-Y = protonated Y zeolite; USY = ultra-stable Y zeolite; H-BETA = protonated BETA zeolite.
[b] Calculated under the specific temperature based on the total Ni metal in catalyst.
[c] Calculated based on Arrhenius plots in the temperature range 553 − 593 K.

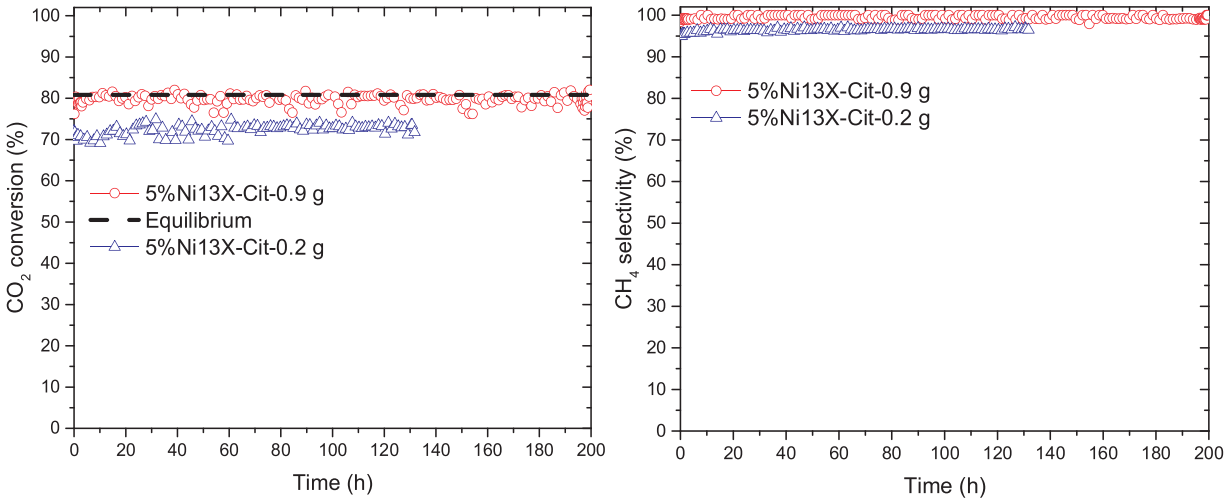

Fig. 10. CO_2 conversion (left) and CH_4 selectivity (right) of 5%Ni13X-Cit at 360 °C with 150 mL/min N_2, 40 mL/min H_2, 10 mL/min CO_2.

[38].

Overall (Fig. 8), the CO_2 conversion orders are 5%Ni13X-Cit > 5% Ni13X-Ace > 5%Ni13X-Nit, 5%Ni5A-Ace ≈ 5%Ni5A-Nit > 5%Ni5A-Cit. The CH_4 selectivity orders are 5%Ni13X-Cit > 5%Ni13X-Ace > 5% Ni13X-Nit, 5%Ni5A-Cit ≈ 5%Ni5A-Ace > 5%Ni5A-Nit. Ni13X zeolite catalysts made from nickel citrate and nickel acetate display a better conversion than all the other catalysts in the temperature range 240 − 440 °C. Even though most 5A zeolite supported catalysts display high CH_4 selectivity at low temperature (selectivity (100-x)% means x% CO is formed), the performance (conversion and selectivity) of the 5A zeolite supported catalysts are inferior to those of 5%Ni13X-Cit and 5% Ni13X-Ace, at temperatures around 320 − 360 °C. This may be attributed to a combination of acidity and particle size. Particles are formed inside the pores of 13X and they naturally possess a narrower particle size distribution compared to the particles, which are formed on the surface of the zeolite particles. Weak acidity inside 13X favors the interaction with CO_2. Additionally, according to the CO_2 methanation mechanism, more cations (e.g., Na^+, Mg^{2+}) in 13X zeolite may contribute the higher CO_2 adsorption thereby higher higher conversion during CO_2 methanation [54].

For Ni 5A zeolite catalysts, more Ni was located outside the 5A crystal surface and not homogenously distributed as with the Ni 13X zeolite catalysts (Fig. 3). The small particles dispersed homogenously on zeolite are believed to be the most effective in CO_2 methanation. Additionally, the catalyst selectivity for CH_4 may be associated with the weak acidity of catalysts [55]. 5%Ni13X-Cit has the highest weak acidity, which may be one reason why it has the highest CH_4 selectivity among the Ni- 13X catalysts prepared with different Ni precursors. 5% Ni5A-Nit, 5%Ni5A-Cit and 5%Ni5A-Ace have a close value of weak acidity (Fig. 6), which may result in the close CH_4 selectivity values.

In conclusion, nickel citrate is clearly an interesting Ni precursor for preparing Ni13X zeolite catalysts with the evaporation impregnation method for CO_2 methanation.

The catalyst's calcination temperature is an important factor for catalyst activity, since the calcination procedure is a key factor for the growth of metal sites. Too high temperatures may lead to the sintering of the active metal and reduce the number of active sites. The calcination temperature influenced the conversion of CO_2 and selectivity towards CH_4. An optimum was found at 400 °C as displayed in Fig. 9 as higher or lower temperature resulted in lowered activity and selectivity.

3.2.2. Catalyst stability

The catalyst stability in conversion and selectivity experiments were carried out in the same fixed bed reactor system. The CO_2 conversion and CH_4 selectivity of 5%Ni13X-Cit at 360 °C are shown in Fig. 10 for two different catalyst loadings (0.2 g and 0.9 g). The experiment employing a lower catalyst amount was performed to decrease the conversion below the equilibrium. The results for conversion and selectivity are similar to its counterpart in Fig. 8, taking into account that the temperature in Fig. 10 is fixed. 5%Ni13X-Cit had an excellent stability at 360 °C and it displayed high CH_4 selectivity (above 96%).

4. Conclusions

Ni- modified 13X and 5A zeolite catalysts were synthesized using the evaporation impregnation method. The effect of Ni precursors and calcination temperature on the physico-chemical properties, and the catalytic performance in CO_2 methanation were investigated. The physico-chemical properties of the 13X and 5A zeolite, and Ni modified zeolite catalysts were characterized using XRD, SEM-EDX, TEM, STEM-EDX, N_2 physisorption, H_2-TPR and TPD-NH_3. The physico-chemical characterization results show that the crystal structure of 13X and 5A zeolites stays intact with all precursors. Nickel citrate combined with a rather low calcination temperature leads to Ni modified 13X and 5A zeolite catalysts which can be easily reduced at lower temperature compared to the other Ni 13X and 5A zeolite catalysts made with acetate and nitrate. The 13X supported catalysts outperformed the ones synthesized with 5A mainly due to the better penetration of the metal precursors into the zeolite structure. The nickel citrate precursor resulted in better dispersion compared to nitrate and acetate, which resulted also in better performance. 5%Ni13X-cit zeolite catalyst prepared with nickel citrate showed high activity and CH_4 selectivity in the Sabatier reaction at remarkably low temperatures and the catalyst displayed good stability. The current work clearly shows how the selection of precursor can influence the properties of a nickel modified catalyst.

CRediT authorship contribution statement

Liangyuan Wei: Conceptualization, Software, Investigation, Formal analysis, Data curation, Visualization, Writing - original draft. **Wim Haije:** Conceptualization, Investigation, Methodology, Supervision, Writing - review & editing. **Narendra Kumar:** Methodology, Investigation, Formal analysis, Resources, Supervision, Writing - review & editing. **Janne Peltonen:** Investigation. **Markus Peurla:** Investigation. **Henrik Grenman:** Conceptualization, Methodology, Resources, Supervision, Project administration, Funding acquisition, Writing - review & editing. **Wiebren de Jong:** Resources, Supervision, Writing - review & editing.

Declaration of Competing Interest

The authors declare that they have no known competing financial interests or personal relationships that could have appeared to influence the work reported in this paper.

Acknowledgments

The research work is a part of the activities of process and energy department in Delft University of Technology and the Johan Gadolin Process Chemistry Centre. The authors acknowledge the financial support from Åbo Akademi University, The Finnish Society of Science and Letters for Liangyuan's visiting at Turku, the authors also acknowledge the PhD scholarship awarded to Liangyuan Wei by the China Scholarship Council (CSC).

Appendix A. Supplementary data

Supplementary material related to this article can be found, in the online version, at doi:https://doi.org/10.1016/j.cattod.2020.05.025.

References

[1] H.Q. Yang, Z.H. Xu, M.H. Fan, R. Gupta, R.B. Slimane, A.E. Bland, I. Wright, Progress in carbon dioxide separation and capture: a review, J. Environ. Sci. 20 (2008) 14–27.
[2] C. Shuai, L. Shen, L. Jiao, Y. Wu, Y. Tan, Identifying key impact factors on carbon emission: evidences from panel and time-series data of 125 countries from 1990 to 2011, Appl. Energy 187 (2017) 310–325.
[3] F.A. Rahman, M.M.A. Aziz, R. Saidur, W.A.W.A. Bakar, M.R. Hainin, R. Putrajaya, N.A. Hassan, Pollution to solution: capture and sequestration of carbon dioxide (CO_2) and its utilization as a renewable energy source for a sustainable future, Renew. Sustain. Energy Rev. 71 (2017) 112–126.
[4] M.E. Boot-Handford, J.C. Abanades, E.J. Anthony, M.J. Blunt, S. Brandani, N. Mac Dowell, J.R. Fernández, M.-C. Ferrari, R. Gross, J.P. Hallett, Carbon capture and storage update, Energy Environ. Sci. 7 (2014) 130–189.
[5] D.M. Reiner, Learning through a portfolio of carbon capture and storage demonstration projects, Nat. Energy 1 (2016) 15011.
[6] K.Z. House, A.C. Baclig, M. Ranjan, E.A. van Nierop, J. Wilcox, H.J. Herzog, Economic and energetic analysis of capturing CO_2 from ambient air, Proc. Nat. Acad. Sci. 108 (2011) 20428–20433.
[7] L. Wei, H. Yang, B. Li, X. Wei, L. Chen, J. Shao, H. Chen, Absorption-enhanced steam gasification of biomass for hydrogen production: effect of calcium oxide addition on steam gasification of pyrolytic volatiles, Int. J. Hydrogen Energ. 39 (2014) 15416–15423.
[8] B. Li, H. Yang, L. Wei, J. Shao, X. Wang, H. Chen, Hydrogen production from agricultural biomass wastes gasification in a fluidized bed with calcium oxide enhancing, Int J. Hydrogen Energ. 42 (2017) 4832–4839.
[9] J. Wang, K. Sakanishi, I. Saito, T. Takarada, K. Morishita, High-yield hydrogen production by steam gasification of HyperCoal (ash-free coal extract) with potassium carbonate: comparison with raw coal, Energy Fuels 19 (2005) 2114–2120.
[10] H.J. Pasman, W.J. Rogers, Risk assessment by means of Bayesian networks: a comparative study of compressed and liquefied H_2 transportation and tank station risks, Int. J. Hydrogen Energy 37 (2012) 17415–17425.
[11] M. Gotz, J. Lefebvre, F. Mors, A.M. Koch, F. Graf, S. Bajohr, R. Reimert, T. Kolb, Renewable power-to-gas: a technological and economic review, Renew. Energy 85 (2016) 1371–1390.
[12] P. Frontera, A. Macario, M. Ferraro, P. Antonucci, Supported catalysts for CO_2 methanation: a review, Catalysts 7 (2017) 59.
[13] T. Schaaf, J. Grünig, M.R. Schuster, T. Rothenfluh, A. Orth, Methanation of CO_2-storage of renewable energy in a gas distribution system, Energy Sustain. Soc. 4 (2014) 2.
[14] A. Borgschulte, N. Gallandat, B. Probst, R. Suter, E. Callini, D. Ferri, Y. Arroyo, R. Erni, H. Geerlings, A. Züttel, Sorption enhanced CO_2 methanation, Phys. Chem. Chem. Phys. 15 (2013) 9620–9625.
[15] S. Walspurger, G.D. Elzinga, J.W. Dijkstra, M. Sarić, W.G. Haije, Sorption enhanced methanation for substitute natural gas production: experimental results and thermodynamic considerations, Chem. Eng. J. 242 (2014) 379–386.
[16] A. Borgschulte, E. Callini, N. Stadie, Y. Arroyo, M.D. Rossell, R. Erni, H. Geerlings, A. Züttel, D. Ferri, Manipulating the reaction path of the CO_2 hydrogenation reaction in molecular sieves, Catal. Sci. Technol. 5 (2015) 4613–4621.
[17] R. Delmelle, R.B. Duarte, T. Franken, D. Burnat, L. Holzer, A. Borgschulte, A. Heel, Development of improved nickel catalysts for sorption enhanced CO_2 methanation, Int. J. Hydrogen Energ. 41 (2016) 20185–20191.
[18] S. Ronsch, J. Schneider, S. Matthischke, M. Schluter, M. Gotz, J. Lefebvre, P. Prabhakaran, S. Bajohr, Review on methanation - from fundamentals to current projects, Fuel 166 (2016) 276–296.
[19] W. Wei, G. Jinlong, Methanation of carbon dioxide: an overview, Front. Chem. Sci. Eng. 5 (2011) 2–10.
[20] S.F. He, Q.S. Jing, W.J. Yu, L.Y. Mo, H. Lou, X.M. Zheng, Combination of CO_2 reforming and partial oxidation of methane to produce syngas over Ni/SiO_2 prepared with nickel citrate precursor, Catal. Today 148 (2009) 130–133.
[21] S.F. He, Z.Q. Mei, N.S. Liu, L. Zhang, J.C. Lu, X.F. Li, J. Wang, D.D. He, Y.M. Luo, Ni/SBA-15 catalysts for hydrogen production by ethanol steam reforming: effect of nickel precursor, Int. J. Hydrogen Energ. 42 (2017) 14429–14438.
[22] L.A. Chick, L.R. Pederson, G.D. Maupin, J.L. Bates, L.E. Thomas, G.J. Exarhos, Glycine-nitrate combustion synthesis of oxide ceramic powders, Mater. Lett. 10 (1990) 6–12.
[23] B. Delmon, Preparation of heterogeneous catalysts, J. Therm. Anal. Calorim. 90 (2007) 49–65.
[24] H.M. Zhang, Y. Teraoka, N. Yamazoe, Preparation of perovskite-type oxides with large surface-area by citrate process, Chem. Lett. 16 (1987) 665–668.
[25] L. Li, J. Zheng, Y.F. Liu, W. Wang, Q.S. Huang, W. Chu, Impacts of SiC carrier and nickel precursor of NiLa/support catalysts for CO_2 selective hydrogenation to Synthetic Natural Gas (SNG), Chemistryselect 2 (2017) 3750–3757.
[26] J.M. NEWSAM, The zeolite cage structure, Science 231 (1986) 1093–1099.
[27] J.M. Adams, D.A. Haselden, The structure of dehydrated zeolite 5A (SiAl = 1.02) by neutron profile refinement, J. Solid State Chem. 51 (1984) 83–90.
[28] J. Hunger, I.A. Beta, H. Böhlig, C. Ling, H. Jobic, B. Hunger, Adsorption structures of water in NaX studied by DRIFT spectroscopy and neutron powder diffraction, J. Phys. Chem. B 110 (2006) 342–353.
[29] L. Joos, J.A. Swisher, B. Smit, Molecular simulation study of the competitive adsorption of H_2O and CO_2 in zeolite 13X, Langmuir 29 (2013) 15936–15942.
[30] I. Graça, L.V. González, M.C. Bacariza, A. Fernandes, C. Henriques, J.M. Lopes, M.F. Ribeiro, CO_2 hydrogenation into CH_4 on NiHNaUSY zeolites, Appl. Catal. B 147 (2014) 101–110.
[31] A. Luengnaruemitchai, A. Kaengsilalai, Activity of different zeolite-supported Ni catalysts for methane reforming with carbon dioxide, Chem. Eng. J. 144 (2008) 96–102.
[32] C. Zhang, Y.M. Chai, C.G. Liu, Effect of different precursor species on the metal dispersion of a Ni/gamma-Al_2O_3 adsorbent for sulfur adsorption, Appl. Petrochem. Res. 7 (2017) 33–40.
[33] F. Li, X.D. Yi, W.P. Fang, Effect of organic nickel precursor on the reduction performance and hydrogenation activity of Ni/Al_2O_3 catalysts, Catalysis Lett. 130 (2009) 335–340.
[34] E.R. Still, P. Wikberg, Solution studies of systems with polynuclear complex formation. 2. The nickel(II) citrate system, Inorg. Chim. Acta Rev. 46 (1980) 153–155.
[35] T.B. Field, J.L. McCourt, W.A.E. McBryde, Composition and stability of Iron and copper citrate complexes in aqueous solution, Can. J. Chem. 52 (1974) 3119–3124.
[36] W. Brockner, C. Ehrhardt, M. Gjikaj, Thermal decomposition of nickel nitrate hexahydrate, $Ni(NO_3)_2{\cdot}6H_2O$, in comparison to $Co(NO_3)_2{\cdot}6H_2O$ and $Ca(NO_3)_2{\cdot}4H_2O$, Thermochim. Acta 456 (2007) 64–68.
[37] S. Abelló, C. Berrueco, D. Montané, High-loaded nickel–alumina catalyst for direct CO_2 hydrogenation into synthetic natural gas (SNG), Fuel 113 (2013) 598–609.
[38] S. Abate, K. Barbera, E. Giglio, F. Deorsola, S. Bensaid, S. Perathoner, R. Pirone, G. Centi, Synthesis, characterization, and activity pattern of Ni–Al hydrotalcite catalysts in CO_2 methanation, Ind. Eng. Chem. Res. 55 (2016) 8299–8308.
[39] D.J. Lensveld, J.G. Mesu, A.J. Van Dillen, K.P. de Jong, Synthesis and characterisation of MCM-41 supported nickel oxide catalysts, Microporous Mesoporous Mater. 44 (2001) 401–407.
[40] H. Zheng, L. Han, H. Ma, Y. Zheng, H. Zhang, D. Liu, S. Liang, Adsorption characteristics of ammonium ion by zeolite 13X, J. Hazard. Mater. 158 (2008) 577–584.
[41] C.R. Melo, H.G. Riella, N.C. Kuhnen, E. Angioletto, A.R. Melo, A.M. Bernardin, M.R. da Rocha, L. da Silva, Synthesis of 4A zeolites from kaolin for obtaining 5A zeolites through ionic exchange for adsorption of arsenic, Mater. Sci. Eng. B 177 (2012) 345–349.
[42] S. Sun, N. Tsubaki, K. Fujimoto, The reaction performances and characterization of Fischer–Tropsch synthesis Co/SiO_2 catalysts prepared from mixed cobalt salts, Appl. Catal. A Gen. 202 (2000) 121–131.
[43] K.G. Fang, J. Ren, Y.H. Sun, Effect of nickel precursors on the performance of Ni/AlMCM-41 catalysts for n-dodecane hydroconversion, J. Mol. Catal. A-Chem. 229 (2005) 51–58.
[44] X.F. Yang, A.Q. Wang, B.T. Qiao, J. Li, J.Y. Liu, T. Zhang, Single-atom catalysts: a new frontier in heterogeneous catalysis, Acc. Chem. Res. 46 (2013) 1740–1748.
[45] M. Suzuki, K. Tsutsumi, H. Takahashi, Characterization and catalytic activity of nickel-zeolite catalysts. I. Reduction properties of nickel ions in zeolites, Zeolites 2 (1982) 51–58.
[46] Ö. Yavuz, Y. Altunkaynak, F. Güzel, Removal of copper, nickel, cobalt and manganese from aqueous solution by kaolinite, Water Res. 37 (2003) 948–952.
[47] R. Shannon, Revised effective ionic radii and systematic studies of interatomic distances in halides and chalcogenides, Acta Crystallogr. Sect. A 32 (1976) 751–767.
[48] P.D. Jadhav, R.V. Chatti, R.B. Biniwale, N.K. Labhsetwar, S. Devotta, S.S. Rayalu, Monoethanol amine modified zeolite 13X for CO_2 adsorption at different temperatures, Energy Fuels 21 (2007) 3555–3559.
[49] H.H. Yong, H.C. Park, Y.S. Kang, J. Won, W.N. Kim, Zeolite-filled polyimide membrane containing 2,4,6-triaminopyrimidine, J. Membr. Sci. 188 (2001) 151–163.
[50] G.R. Hedwig, J.R. Liddle, R.D. Reeves, Complex formation of nickel (II) ions with citric acid in aqueous solution: a potentiometric and spectroscopic study, Aust. J. Chem. 33 (1980) 1685–1693.
[51] S.-C. Ho, T.-C. Chou, The role of anion in the preparation of nickel catalyst detected by TPR and FTIR spectra, Ind. Eng. Chem. Res. 34 (1995) 2279–2284.
[52] B.M. Abu-Zied, A.M. Asiri, An investigation of the thermal decomposition of nickel

citrate as a precursor for NiNiO composite nanoparticles, Thermochim. Acta 649 (2017) 54–62.
[53] J.C. De Jesus, I. González, A. Quevedo, T. Puerta, Thermal decomposition of nickel acetate tetrahydrate: an integrated study by TGA, QMS and XPS techniques, J. Mol. Catal. A Chem. 228 (2005) 283–291.
[54] A. Westermann, B. Azambre, M.C. Bacariza, I. Graca, M.F. Ribeiro, J.M. Lopes, C. Henriques, Insight into CO_2 methanation mechanism over NiUSY zeolites: an operando IR study, Appl. Catal. B-Environ. 174 (2015) 120–125.
[55] M.C. Sánchez-Sánchez, R.M. Navarro, J.L.G. Fierro, Ethanol steam reforming over Ni/MxOy–Al_2O_3 (M = Ce, La, Zr and Mg) catalysts: influence of support on the hydrogen production, Int. J. Hydrogen Energ. 32 (2007) 1462–1471.
[56] M.A.A. Aziz, A.A. Jalil, S. Triwahyono, M.W.A. Saad, CO_2 methanation over Ni-promoted mesostructured silica nanoparticles: influence of Ni loading and water vapor on activity and response surface methodology studies, Chem. Eng. J. 260 (2015) 757–764.
[57] P.F. Zhu, Q.J. Chen, Y. Yoneyama, N. Tsubaki, Nanoparticle modified Ni-based bimodal pore catalysts for enhanced CO_2 methanation, RSC Adv. 4 (2014) 64617–64624.
[58] M.A.A. Aziz, A.A. Jalil, S. Triwahyono, R.R. Mukti, Y.H. Taufiq-Yap, M.R. Sazegar, Highly active Ni-promoted mesostructured silica nanoparticles for CO_2 methanation, Appl. Catal. B-Environ. 147 (2014) 359–368.
[59] G. Garbarino, D. Bellotti, P. Riani, L. Magistri, G. Busca, Methanation of carbon dioxide on Ru/Al_2O_3 and Ni/Al_2O_3 catalysts at atmospheric pressure: catalysts activation, behaviour and stability, Int. J. Hydrogen Energ. 40 (2015) 9171–9182.
[60] A. Quindimil, U. De-La-Torre, B. Pereda-Ayo, J.A. González-Marcos, J.R. González-Velasco, Ni catalysts with La as promoter supported over Y- and BETA- zeolites for CO_2 methanation, Appl. Catal. B 238 (2018) 393–403.